Journal of King Saud University - Science 36 (2024) 103256

HOSTED BY

Contents lists available at ScienceDirect

Journal of King Saud University - Science

journal homepage: www.sciencedirect.com

Physiochemical characterization of *Glycyrrhiza* mediated bioengineered palladium nanoparticles (PdNPs), their anti-proliferative and other biomedical applications

Najlaa S. Al-Radadi

Department of Chemistry, Faculty of Science, Taibah University, P.O. Box 30002, Al-Madinah Al-Munawarah 14177, Saudi Arabia

ARTICLE INFO

Keywords:
Palladium Nanoparticles
Synthesis
Anticancer
Glycyrrhizin acid
Antibacterial

ABSTRACT

The study used *licorice root* leaf extract to synthesize palladium nanoparticles (PdNPs) that demonstrate long-term stability, lower toxicity, and enhanced penetration into specific target cells. The optimal conditions (temperature, pH, and time) were maintained to synthesize regular, spherical, and homogenous nanoparticles. The PdNPs were characterized by Energy dispersive X-ray spectroscopy, UV–Visible spectroscopy, High-resolution Transmission electron microscope, X-ray diffraction, Particle-Size Distribution, Fourier Transform Infrared Spectroscopy, X-ray photoelectron spectroscopy, and Zeta potential analysis. The biosynthetic PdNPs used ABTS and DPPH assay to demonstrate strong antioxidant potential with maximal inhibition. PdNPs hindered the growth of *Escherichia coli*, *Staphylococcus aureus*, *Bacillus subtilis*, and *Pseudomonas aeruginosa* with zone of inhibition that was 20–25 ± 0.22 mm. PdNPs showed anti-Alzheimer activity by suppression of acetylcholinesterase and butyryl cholinesterase enzymes. Furthermore, the minimum anti-proliferative concentration of PdNPs was detected against MCF-7 and HCT-116 which was 44.4 at 6.58 µg/mL, respectively. Thus, PdNPs have proved to be an effective therapeutic agent for drug delivery and other biomedical applications in the pharmaceutical industry.

1. Introduction

Glycyrrhiza belongs to Fabaceae sub-family of *Leguminosae* family (Goyal et al., 2020). *Licorice root* is a widely used plant in Ayurvedic medicine, known for its ethano-pharmacological value in treating various disorders (Thakur and Raj, 2017). *Licorice root* contains amines like Lin 12-keto-triterpensaponins and glycyrrhizin, which inhibit 11β-hydroxysteroid dehydrogenase and act as an anti-inflammatory agent (Wittschier et al., 2009).

Licorice root contains over 20 triterpenoids and 300 flavonoids, including active compounds like glycyrrhizin, licochalcone A, 18β-glycyrrhetinic acid, glabridin, liquiritigenin, and licochalcone that may have potent antiviral and antimicrobial properties (Al-Radadi 2021a). *Licorice root* extracts have been used in Japan to treat chronic hepatitis, HIV, cytomegalovirus (CMV), and herpes simplex. *Licorice root* is rich in glycyrrhizin and saponin and is used to treat rheumatism without cortisone's harmful effects It offers anti-inflammatory, antioxidant, antimalarial, antispasmodic, diuretic, and sedative properties (Al-Radadi 2022a). Herbal medicines exhibit antifungal, antihepatotoxic, antiviral, and anxiolytic properties to enhance cognitive performance and alleviate Alzheimer's disease (Chakravarthi and Avadhani, 2013).

Nanotechnology has improved the therapeutic index in treating diseases like cancer which provides new treatments for antiviral, anticancer, antidiabetic, and antiallergic (Al-Radadi., 2022b, Al-Radadi., 2022c, Al-Radadi., 2022d). Noble metal (Ag, Pd, Pt, and Au) nanoparticles (NPs) are utilized in various fields such as biomedicine, biosensing, electronics, drug administration, and surface-enhanced Raman scattering (SERS) (Al-Radadi., 2018, Al-Radadi. and Abu-Dief., 2022, Al-Radadi and Al-Youbi., 2018a, Al-Radadi., 2019, Al-Radadi and Adam., 2020, Al-Radadi., 2021b). These nanoparticles demonstrate intensive application because of their unique features at the nanometric scale (Al-Radadi and Al-Youbi., 2018b; Al-Radadi., 2023). Different methods are employed for synthesizing nanoparticles with a limited size distribution, affective physicochemical parameters, and requires significant effort to achieve optimal size, shape, and content (Al-Radadi et al., 2024).

The intriguing characteristics of palladium oxide nanoparticles (PdONPs) are frequently used in the building of ships, construction of roads, and biological application including their rustproof, antibacterial, and anti-algae capabilities. Moreover, the small-sized particles enhance

E-mail address: nsa@taibahu.edu.sa.

https://doi.org/10.1016/j.jksus.2024.103256
Received 16 October 2023; Received in revised form 12 May 2024; Accepted 12 May 2024
Available online 13 May 2024

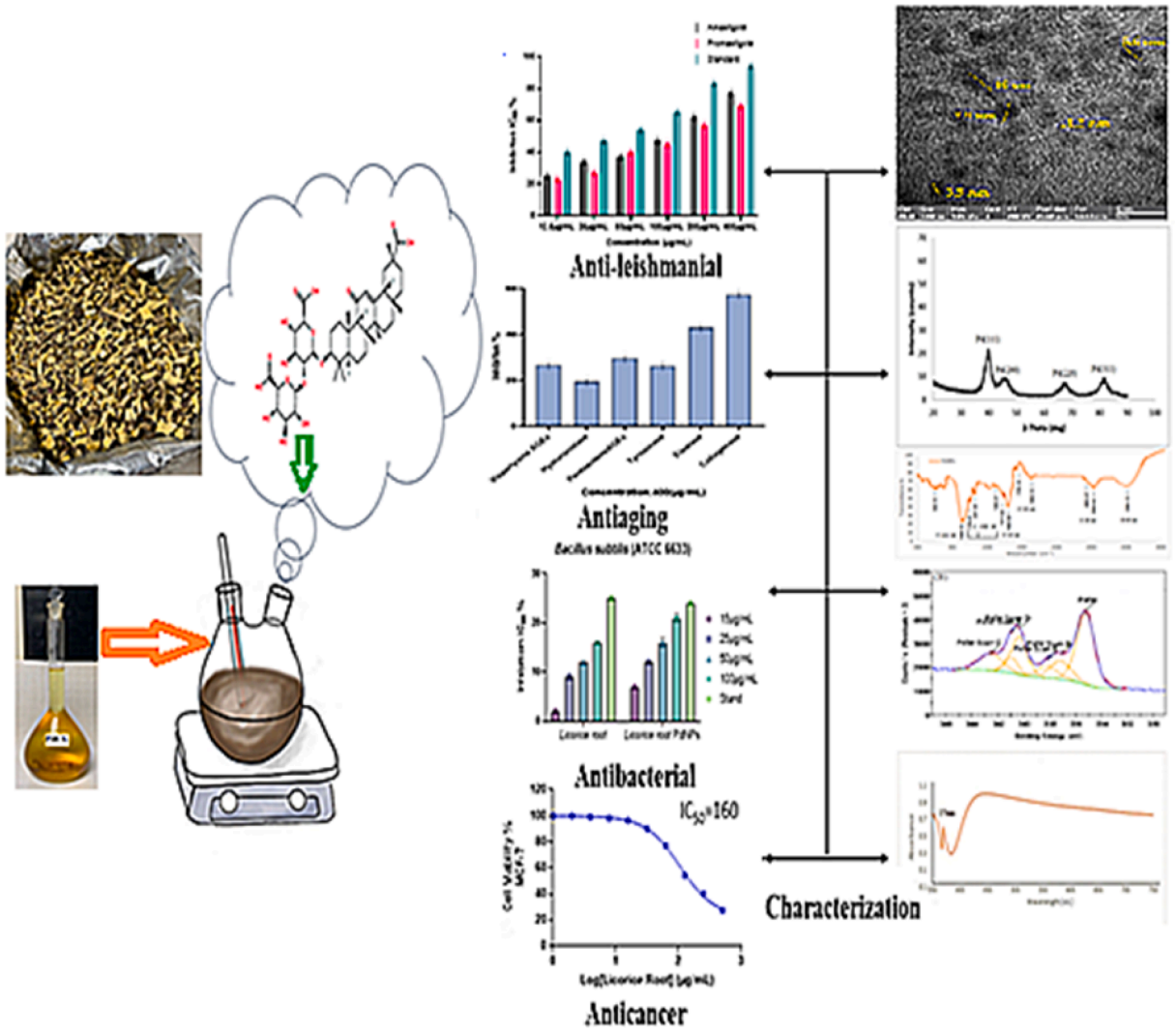

Fig. 1. Schematic diagram of green synthesized PdNPs containing Glycyrrhiza extract: characterization and essential biological applications. (For interpretation of the references to color in this figure legend, the reader is referred to the web version of this article.)

the properties of drug carriers, antioxidant, antimicrobial, photothermal agents, hydrogen storage, and sensing agents (Mayedwa et al., 2018).

The synthesis of PdNPs was influenced by electrochemical chemicals, surfactants, and polymers as capping and reducing agents with beneficial catalytic applications (Al-Radadi 2022e; Al-Ahmed et al., 2020). Ecofriendly plant molecules show exceptional catalytic characteristics when binding with PdNPs, due to deformation changes in cellular structure and catalytic components reducing Pd (II). The deposition of PdNPs on cell surfaces and the catalytic activity of bio Pd are influenced by both initial Pd (II) biosorption and subsequent Pd (0) bioreduction (Deplanche et al., 2014).

In the present study, efficient PdNPs were achieved by green source synthesis of nanoparticles. *Licorice root* plant is used for the green method of preparing PdNPs and is an environmentally friendly, non-toxic, and single-step process (Cerqueira et al., 2015). The homogeneous nature of the NPs enhanced the sensitivity, optical, and physical properties of PdNPs. Thus, the goal of the current investigations was to explore the antioxidant, anti-inflammatory, antibiotic, anti-leishmanial, anti-aging, anti-Alzheimer, and anticancer activity as shown in (Fig. 1). Moreover, the biosynthetic method using green sources from *licorice roots* extract has shown to be a feasible and desirable substitution. Therefore, the current study describe the *Licorice root* extracts have been used to synthesize PdNPs. The synthesis of nanoparticles were further confirmed by TEM, XRD, UV–vis, FTIR, EDS, XPS, and zeta potential analysis, and the antibacterial, antioxidant, anti-inflammatory, Anti-leishmanial, Anti-aging, anti-Alzheimer, and anticancer activity were reported first time in detail using *Licorice roots* extracts.

2. Experimental

2.1. Extraction and preparation of licorice root

Licorice root was rinsed with double distilled water to remove any contaminants. An aqueous extract of 5 g of *licorice root* is filtered after being boiled in (70 ml) double distilled water and (20 ml) ethanol. Sodium hydroxide was used to adjust the pH. The extract was filtered and stored for further use.

2.2. Palladium nanoparticle synthesis

Palladium chloride solution ($PdCl_2$) concentrated (2×10^{-3}M) was mixed with (6 mL and 2 mL of *Licorice root* extract). The mixture was kept for 3 h at 100 °C on a magnetic stirrer. After that, the synthesis of PdNPs was confirmed with the color transformation to dark brown which was further validated by UV–Vis analysis, and the solution was filtered and kept at 4 °C for further examination.

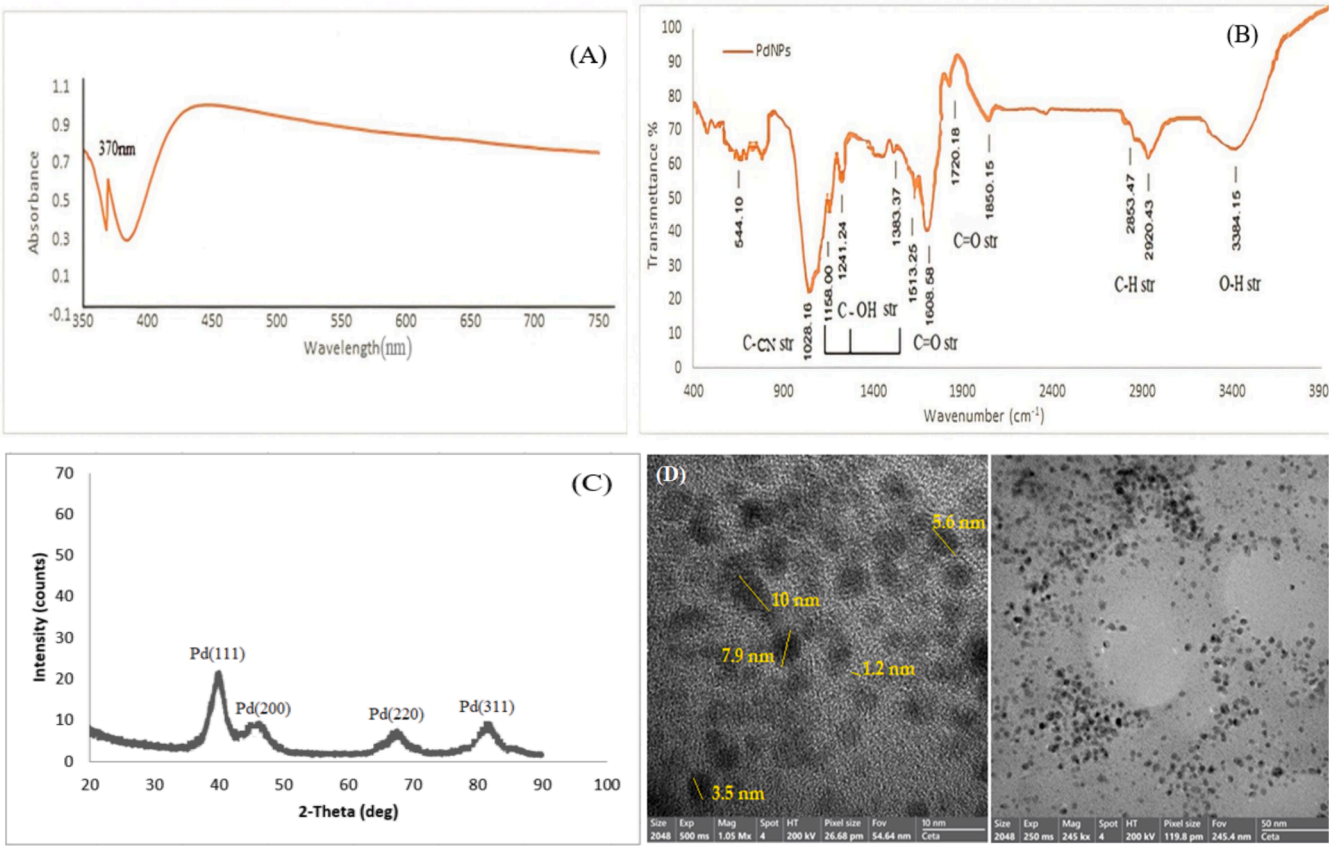

Fig. 2. UV–Visible spectrum of Biosynthesized PdNPs from *Glycyrrhiza* extract **(A)**, FTIR spectra of *Glycyrrhiza*- PdNPs **(B)**, XRD spectrum of PdNPs synthesized by *Glycyrrhiza* extract **(C)**, HR-TEM and TEM image of PdNPs produced by *Glycyrrhiza* extract **(D)**.

2.3. Characterizations of green synthesized PdNPs

PdNPs formation were observed employing UV–Vis spectroscopy with a twin spectrometer at a wavelength of 350 to 700 nm. The Shimadzu XRD instrument was used to characterize powder PdNPs. FTIR (FTIR-Nico-let 6700) was done to establish the functional groups in the range of 400–4000 cm^{-1}. TEM (A JEOL/JEM 2100) set to 90 KV was used to analyze the specific surface area. In contrast to the Zeta potential measurements, the EDX was also performed to determine the elemental composition of PdNPs.

2.4. Biological potential of the PdNPs

2.4.1. Antioxidant assay

The antioxidant potential of PdNPs was examined by DPPH (2,2-diphenyl-1-picrylhydrazyl) and ABTS (2,2′-azino-bis 3-ethylbenzothiazoline-6-sulfonic acid). Different concentrations of PdNPs were used ranging from 10 to 50 μg/mL, followed by dilution with 3 mL of DPPH solution at (0.01 mM). The reaction mixture was shaken and stored in the dark for 30 mins. The wavelength was recorded at 400–750 nm using ascorbic acid as a baseline. The proportions were determined using the following formula:

$$\% \text{ RSA} = \frac{\text{AC} - \text{AT}}{\text{Absorbance of blank}} \times 100.$$

Whereas AT = Absorbance of the Sample,

AC = Control group absorbance and Ascorbic acid were used as the reference.

The ABTS + assay exhibits maximum absorbance at 645–815 nm, indicating discoloration caused by the combination of ABTS solvent and peroxydisulfuric acid. ABTS + spectrophotometrically identifies hydrophilic and hydrophobic antioxidant properties, measuring scavenge free radicals in trolox equivalents that is a water-soluble vitamin E counterpart as a reference.

2.4.2. Anti-inflammatory assay

Murine macrophages RAW264.7 cells were grown in basal medium (DMM) accompanied with penicillin (100 μg/mL), 10 % FBS, 2 mM (glutamide 2,5-Diamino-5-oxopentanoic acid 2-Amino-4-carbamoylbutanoic acid), and streptomycin sulphate (100 μg/mL) in a temperature controlled 5 % of CO_2 in the air. The cells were rinsed in phosphate-buffered saline and then scraped off the flasks using sterile scrappers for passaging and treatment. RAW 264.7 cells ($0.5x10^6$ cells/mL) were planted onto 96 microplate reader substrates and incubated overnight. An inflammatory group of triplicate wells received lipopolysaccharide (LPS) in full culture media at a concentration of 100 mg/mL, whereas non-induced triplicate wells received medium along with the sample. The volumes of the extract increased (6.25–100 μg/mL) and were dissolved on LPS in culture media. The caffeic acid phenacyl ester (CAPE, 5 M) was used as a positive control. Griess test was to measure NOs after 24 h of incubation. The colored diazonium salt was prepared by mixing equal parts culture supernatants and Griess reagent that was recorded at 540 nm after 10 min of incubation. The extract NOs inhibition percent test was compared to the normalized to cell viability and LPS-induced inflammation group using the Alamar Blue TM reduction assay.

2.4.3. Anti-leishmanial assay

Biogenic PdNPs were tested for their anti-leishmanial properties against Leishmania tropica KWH23 amastigote and promastigote growth at Al-Azhar University's Regional Center for Mycology and Biotechnology. The M199 medium, containing 10 % fetal bovine serum, effectively cultured leishmanial pathogens at a density of $1x10^6$ cells per mL. The experiment involved varying PdNPs densities, with the lowest being 12.5 μg/mL and the highest being 400 μg/mL in each sample.

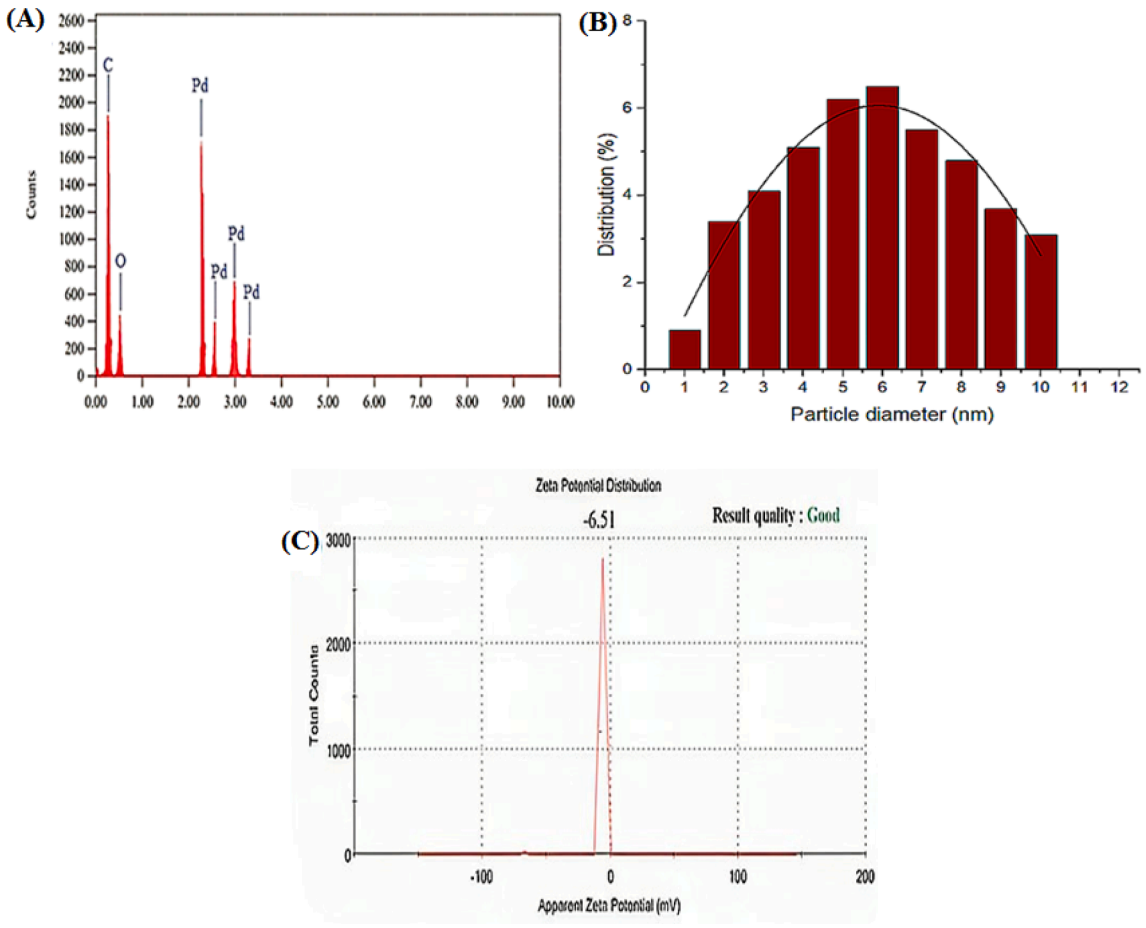

Fig. 3. EDX spectrum **(A)**, size distribution of PdNPs with *Glycyrrhiza* extract **(B)** and Zeta potential of Biosynthesized PdNPs **(C)**.

Leishmania parasites were successfully grown in medium (M199) with 10 % FBS using Mysteclin-F as a control and DMSO in the nullifying sample. The study also used $1x10^6$ cells/mL of Leishmania culture in a 96-well plate in account to select the diluent and was incubated for 72 h at room temperature. Viable colonies were enumerated using a fluorescent microscope. The Table Curve software was utilized to compute IC50 values. Furthermore, the following equation was used to calculate the inhibitory activities.

$$\%\,\text{Inhibition} = [1 - \left\{\frac{\text{Total Absorbance of sample}}{\text{Absorbance of Control sample}}\right\}] \times 100$$

2.4.4. Antibacterial assay

2.4.4.1. Agar well diffusion method. The antibacterial activity of PdNPs were evaluated by the standard agar method. A sterile borer was used to create six wells and tested bacterial isolates were introduced with varying concentrations of *Licorice root* extracts and PdNPs (15 µg/mL, 25 µg/mL, 50 µg/mL, and 100 µg/mL). The samples that were incubated for 24 h at 37 °C were stored overnight with streptomycin as the control. The zone of inhibition (mm) was calculated using a scale.

2.4.5. Anti-Aging assay

2.4.5.1. Anti-AGE formation assay. The synthesis of Vesper lysine AGEs and Pentosidine AGEs was evaluated for their potential as inhibitors. The BSA solution (Sigma Aldrich) was designed by mixing 0.1 MW of PBS (pH 7.4), which included 0.02 % sodium azido, with 0.5 MW of sucrose. After mixing a 20 µg/mL BSA solvent for PdNPs, it was left at room temperature in the dark for 5 days.

2.4.5.2. Tyrosine's assay. The substrate for the tyrosinase assay was L-DOPA (5 mM). PdNPs and the LDOPA diphenol substrate were combined in 100 mL of PBS (50 mM, pH 6.8). The total concentration is then raised to 200 mL infusing 0.2 mg/mL of mushroom extract as a reagent. The percentage inhibition of standard tyrosinase activity is used to measure the PdNPs tyrosinase impact.

2.4.5.3. Elastase assay. This experiment used pancreatic elastase. Following three testing cycles, the percentage of inhibition of the anti-elastase activity relative to the untreated was calculated.

2.4.5.4. Hyaluronidase assay. The hyaluronic acid concentration of 0.03 percent and hydrolytic enzyme units of 1.5 were combined. The hyaluronic acid(undigested form) is dissolved in an acidic plasma proteins mixture (0.1 percent (w/v) BSA), which causes acid to develop. The growth reduction was quantified by anti-hydrogenase activity.

2.4.5.5. Collagenase assay. This test is created on the reaction between collagenase enzyme and chemically synthesized FALGPA. The reaction between 25 µg/mL of test samples and 25 ml of collagenase produced by Clostridium histolyticum was allowed in a 96-well microtiter plate containing pH 7.5 and 25 mL of tricine buffer (with 10 mM $CaCl_2$ and 400 mM NaCl). The solution was incubated in the dark for 20 min, followed by a 25 mL dose of EGCG and 50 mL of FALGPA (1.6 mM) working solution for each well. The experiment was conducted three times, and the percentage of anti-collagenase inhibition in contrast to the control was calculated.

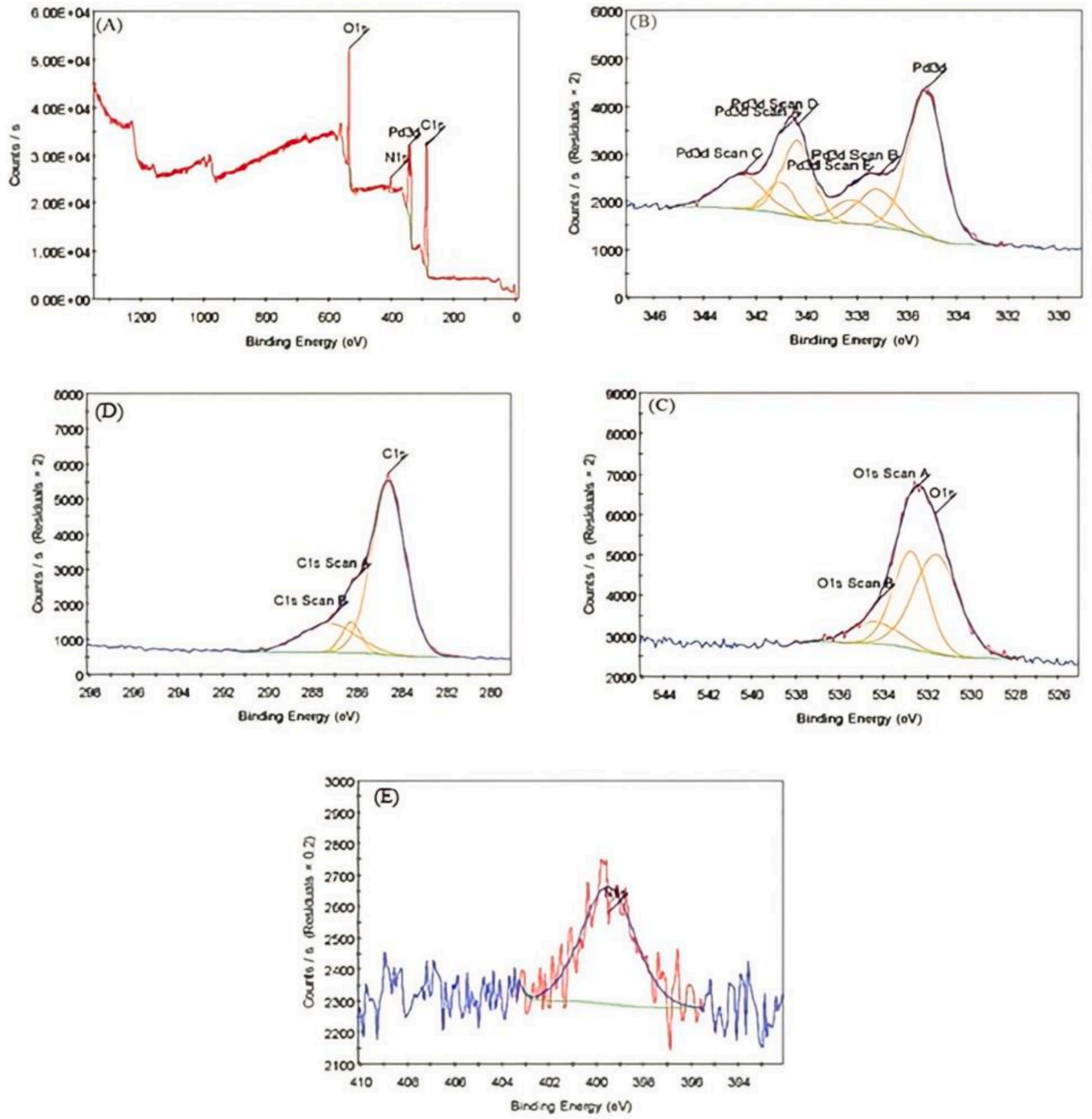

Fig. 4. X-ray photoelectron spectroscopy of PdNPs. A) Cyrstalline Phase of PdNPs, B) Binding Energy of Pd in PdNPs, C) Represnts C1s Peaks, D) Represents O1s Peaks, and E) Represents N1s Peaks.

2.4.6. Anti-Alzheimer's assay

Alzheimer's disease treatments may inhibit the acetylcholinesterase and butyrylcholinesterase catalysts with samples ranging from 25 μg/mL to 400 μg/mL. The Phosphate Buffer Saline was used to disperse the NPs and the final enzyme concentrations in BChE and AChE were 0.01 and 0.03 units/mL, respectively. The solution was prepared in distilled water and stored at 8 °C. BTchI (0.0005 M), DTNB (0.00022 M), and ATchI (0.0005 M) were present and their diffusion coefficient, galantamine, and PdNPs can be used to calculate enzymatic activity and restriction percentage over time.

2.4.7. Anticancer assay

The VACSERA Tissue Culture Unit supplied MCF-7 and HCT-116 cell lines that grown low glucose HCT-116 cells in (MEM) medium and Dulbecco's Modified Eagle medium. Both mediums included 10 % FBS as a dietary additive and were medicated with penicillin/streptomycin solution for protection. The IC_{50} of Dox and (licorice root extract) was calculated by growing MCF-7 or HCT-116 cells in 12-well plates (0–200 M dissolved in DMSO), licorice root (0–400 μg/mL dissolved in DMSO), PdNPs, and licorice root extract (0–400 μg/mL diluted in DMSO) were used to treat the cells. The cells were loaded and incubated for 2 h using an MTT assay, followed by dissolving the formazan crystals

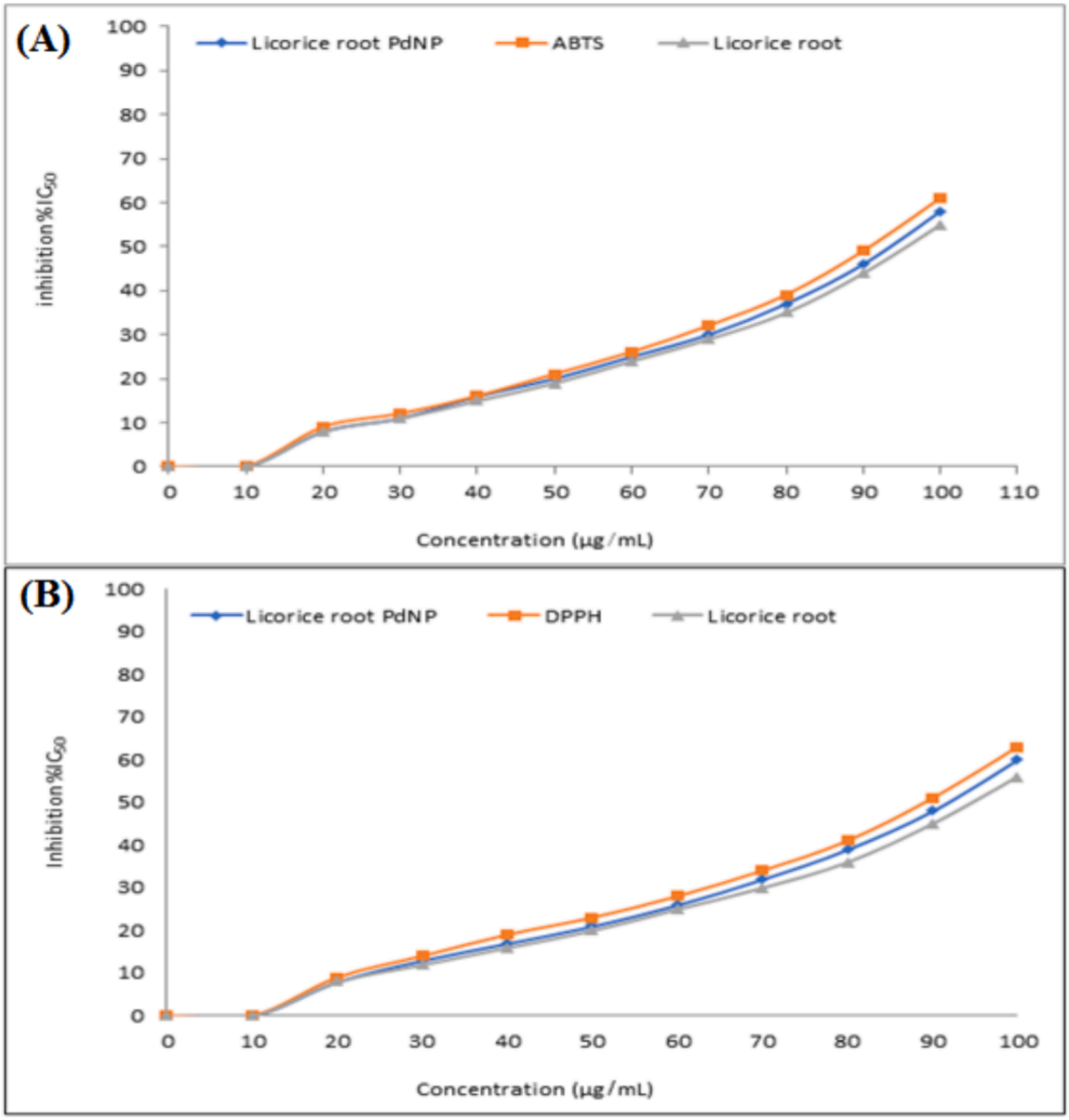

Fig. 5. ABTS free radicals scavenging assay **(A),** and DPPH free radicals scavenging assay of biosynthesized PdNPs **(B)**.

in1 mL of DMSO and determining their optical concentration was determined at 370 nm.

using a colorimetric assay. The CI for each cell were calculated at specific doses using the IC_{50} curves for MCF-7 and HCT-116 cells from the MTT data.

3. Result and discussion

3.1. UV–VIS spectroscopy

PdNPs were obtained by combining *licorice root* extract and palladium dichloride ($PdCl_2$) (1 mL, 2 mL, 4 mL, 5 mL) with *licorice root* extract of (1–8 mL, 8 mL, 6 mL, and 5 mL). PdNPs synthesis was observed when the color of the mixture was gradually changed from black to dark brown after three hours at 100 °C. The ($PdCl_2$) mixture had a clear signal in UV–visible spectroscopy at 370 nm suggesting the existence of Pd^{+2} ions.

(Fig. 2**A)** displays the UV–visible absorption spectrum of PdNPs created with a consistent (4 mL) extract of licorice root. PdNPs production was increased due to the high concentration of $PdCl_2$, as evidenced by UV–visible absorption spectra of PdNPs at 4 mL of extract. The zero Plasmon wavelength strength was seen as the $PdCl_2$ was raised from (1 mL to 2 mL). When the concentration of $PdCl_2$ was increased from 1–8 mL the rise in Plasmon frequency was at 370 nm.

3.2. Fourier-Transform infrared spectroscopy (FT-IR)

FTIR spectrum of solid, liquid, and gas dispersion can easily identify the functional groups of *Licorice root*. FTIR spectra revealed peaks at 3384, 2920, 2853, 1850, 1720, 1608, 1513, 1383, 1241, 1158, 1028, and 544 cm^{-1} as shown in (Fig. 2**B)**. The bending vibration of the C-H bond was observed by two peaks at 2920 cm^{-1} and 2853 cm^{-1}, respectively. The small peaks at 1850 were stretching vibrations of phenolic C = O bonds. The bands at 1513, 1383, and 1158 cm^{-1} correspond to the bending vibrations of C-OH functional group, respectively. The C-N stretching is ascribed to peak 1028 cm^{-1}.

3.3. X-ray diffraction (XRD) analysis

The crystallization of colloidal PdNPs was confirmed by a

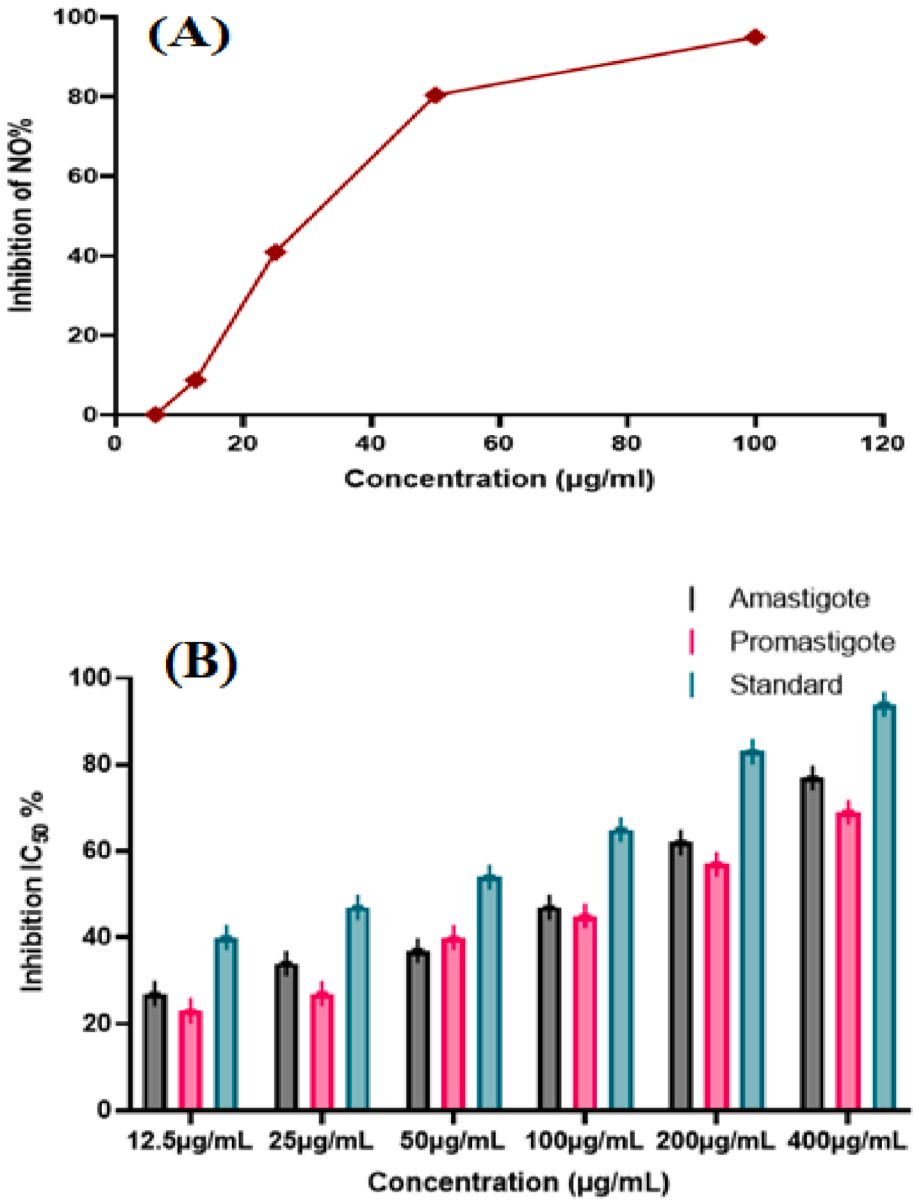

Fig. 6. Anti-inflammatory potential of PdNPs increased with respect to increase in NPs dose **(A),** Anti-leishmanial activity of Biosynthesized PdNPs against *amastigote* and *promastigote* **(B).**

characteristic inversion of the 111, 200, 220, and 311 planes at $2\theta = 40°$, 46.5°, 63°, and 82°, respectively (Fig. 2**C**). The face center cubic geometry of PdNPs was described by the JCDPS standard. The strong band at (1 1 1) of synthesized PdNPs indicates a crystallographic characteristic and is the primary alignment due to its proximity to other surfaces.

3.4. Electron microscopy (TEM) studies

TEM images were captured immediately following the synthesis to determine the shape and size. The diagram in (Fig. 2**D**) shows that PdNPs had a diameter of 10 nm. TEM images show spherical shape PdNPs with diameters ranging from 1.2 to 10 nm, demonstrating that green synthesis produces PdNPs with restricted size (Han et al., 2019), Furthermore, The green synthesis of palladium at room temperature was demonstrated to have relatively small amounts of PdNPs response (Fig. 2**D**).

3.5. Energy-dispersive X-ray spectroscopy

Energy-dispersive X-ray spectroscopy was employed to confirm the presence of Pd in PdNPs. The EDX results in (Fig. 3**A**) demonstrated that NPs are composed of Pd along with C and O elements. The C and O elements were the possible impurities that were inadvertently introduced from the surface molecule of the plant extract during the synthesis. The EDX graph showed strong signals at 2.8 keV, indicating the presence of Pd (Fig. 3**A**). The presence of phytochemicals in *licorice root* indicates compounds like oxygen and carbon. The histogram was used to quantify the nanoparticles size which was 1–10 nm (Fig. 3**B**).

3.6. Zeta potential

The charge distribution of the PdNPs was investigated using zeta potential. The zeta potential was reported to be −6.51 mV (Fig. 3**C**). The observed coefficient values vary from −20 to −30 mV, indicating that the nanoparticles were effectively acceptable for biological applications (Basavegowda et al., 2015).

Table 1
Antibacterial activity (zone of inhibition) from *Glycyrrhiza* and *Licorice root*-PdNPs against Gram positive and Gram-negative bacteria.

Microorganisms	Concentration (µg/mL)	*Glycyrrhiza* extract	PdNPs
Staphylococcus aureus **(ATCC 29213)**	15 µg/mL	1 ± 0.6	9 ± 0.7
	25 µg/mL	5 ± 0.9	12 ± 0.7
	50 µg/mL	10 ± 0.0	17 ± 0.8
	100 µg/mL	14 ± 0.2	20 ± 0.8
	Standard	24 ± 0.6	25 ± 0.6
	Control	0.0 ± 0.0	0.0 ± 0.0
Bacillus subtilis **(ATCC 6633)**	15 µg/mL	1 ± 0.9	7 ± 0.0
	25 µg/mL	9 ± 0.5	12 ± 0.1
	50 µg/mL	12 ± 0.0	16 ± 0.9
	100 µg/mL	16 ± 0.11	21 ± 0.8
	Standard	25 ± 0.3	24 ± 0.2
	Control	0.0 ± 0.0	0.0 ± 0.0
Escherichia coli **(ATCC 25922)**	15 µg/mL	3 ± 0.5	9 ± 0.1
	25 µg/mL	10 ± 0.4	14 ± 0.1
	50 µg/mL	13 ± 0.9	20 ± 0.9
	100 µg/mL	19 ± 0.7	26 ± 0.3
	Standard	23 ± 0.7	24 ± 0.4
	Control	0.0 ± 0.0	0.0 ± 0.0
Pseudomonas aeruginosa **(ATCC 27853)**	15 µg/mL	3 ± 0.1	5 ± 0.0
	25 µg/mL	6 ± 0.0	10 ± 0.8
	50 µg/mL	11 ± 0.1	15 ± 0.7
	100 µg/mL	16 ± 0.2	23 ± 0.6
	Standard	25 ± 0.6	24 ± 0.6
	Control	0.0 ± 0.0	0.0 ± 0.0
Salmonella typhi **(ATCC 6539)**	15 µg/mL	2 ± 0.9	6 ± 0.4
	25 µg/mL	7 ± 0.4	12 ± 0.0
	50 µg/mL	12 ± 0.7	17 ± 0.2
	100 µg/mL	17 ± 0.0	21 ± 0.6
	Standard	25 ± 0.6	23 ± 0.8
	Control	0.0 ± 0.0	0.0 ± 0.0

The diameter (mm) is included in the measured zone of inhibition, Standard Antibiotic (Positive control) and Control (Negative control).

3.7. X-ray photoelectron spectroscopy (XPS) analysis

The XPS analysis of PdNPs revealed the presence of three elements Oxygen (O), Carbon (C), and Nitrogen (N) in their crystalline phase **(**Fig. 4**A)**. The peaks at 534.2, 401.35, and 286.71 eV were assigned to O1 s, N1 s and C1 s, respectively. Fig. 4**B** showed the Pd binding energy of PdNPs at 340.99 to 337.15 eV with a band gap of 3.84 eV. Fig. 4**C** represents the C1s peaks at 284.58 eV, 286.24 eV, 287.26 eV which refers to electron emission evolved from the (C = C), (C = 0), and (C = O) of carbonyl groups during the synthesis. In Fig. 4**D** the O1s peaks at 531.58 eV, 532.74 eV, and 543.37 eV represents the (O-H), (C = O), and (C-OH) in the biological samples. Fig. 4**E** represents the N1s peak at 399.5 eV assigned to C-N. Therefore, the XPS results confirmed the successful preparation of PdNPs (Al-Radadi., 2022e).

3.8. Biological activity

3.8.1. Antioxidant activity by ABTS and DPPH

The DPPH and ABTS assays were used to assess the antioxidant activity of PdNPs. The IC_{50} value of ABTS, *licorice root* extract, and PdNPs were 55 %, 65 %, and 59 % at 100 µg/mL, respectively **(**Fig. 5**A)**, The IC_{50} values of DPPH, *licorice root* extract, and PdNPs were 52 %, 64 %, and 61 % at 100 µg/mL.

3.8.1.1. Antioxidant activity. The DPPH and ABTS activity showed the antioxidant potential of *Licorice root* extract. The results revealed that ABTS and DPHH activity was gradually increased from 0 to 61 % at NPs doses of 10 to 100 µg/mL respectively, as illustrated in **(**Fig. 5**A, B).** The findings showed that the PdNPs synthesized from *licorice root* extract have large number of macromolecules that can scavenge free radicals and contribute strong antioxidant activity.

3.8.2. Anti-inflammatory activity

The study utilized Fecosterol's RAW 264.7 macrophages and their biochemical processes to enhance the anti-inflammatory properties of organic products. The pathogenic components LPS trigger cell activation which releases pro-inflammatory mediators such as IL-1, TNF-a, IL-12, IL-6, COX1, iNOS, COX2, and chemokines. The LPS treatment causes murine monocyte-macrophage RAW 264.7 cells to produce acute cytokines indicating a potential anti-inflammatory drug. PdNPs showed anti-inflammatory potential of 8.73 %, 40.96 %, 80.42 %, and 95.01 % at concentrations of 12.5, 25, 50, and 100 µg/mL as shown in Fig. 6**A**. It was observed that the anti-inflammatory activity increased by increasing the concentration of nanoparticles.

3.8.3. Anti-leishmanial activity

In this analysis, PdNPs were investigated for anti-leishmanial effectiveness. Fig. 6**B** indicates both motile and non-motile forms of the parasite that are strongly suppressed by biosynthesized PdNPs. The maximum inhibition values for promastigote and amastigote were 77 ± 0.10 and 69 ± 0.25 at 400 µg/mL with IC50 values of 169 µg/mL and 175 µg/mL, respectively.

3.8.4. Antibacterial activity

Licorice root-PdNPs showed maximum inhibition zone against *Escherichia coli, Staphylococcus aureus, Bacillus subtilis,* and *Pseudomonas aeruginosa* at concentrations of 15 µg/mL to 100 µg/mL (Perveen et al., 2021). The maximum zone of inhibition were observed at 17 ± 0.0 mm for *S. aureus* and *B. subtilis* and 19 ± 0.7 mm for *E. coli* and *S. typhi*, the ZOI was 14 ± 0.2 mm for *S. aureus* and *B. subtilis*, 16 ± 0.11 mm ZOI was observed for *P. aeruginosa* and *B. subtilis* at maximum concentration as listed in Table 1. At a high concentration PdNPs inhibited the growth of all the microorganisms as shown in Fig. 7.

3.8.5. Anti-aging activity

The study evaluated the anti-aging properties of *licorice root* interlaced with PdNPs, determining their in vitro potency against glucanase, tyrosinase, hyaluronidase, and elastase at 400 µg/mL concentrations. The degradation of extrinsic tissue proteins in the dermal layer, primarily caused by collagenase, hyaluronidase, and elastase-like enzymes, leads to severe wrinkles and skin elasticity issues. PdNPs were found to be dose-dependent inhibition against Visperlysine, Hyaluronidase, Pentosidene, Tyrosinase, Elastase, and Collagenase that was 26.8 ± 0.42, 19.70 ± 0.83, 29.80 ± 0.54, 26.6 ± 0.82, 43.2 ± 0.57, 57.6 ± 0.61 % at 400 µg/mL of concentration, respectively **(**Fig. 8**A)**.

3.8.6. Anti-Alzheimer's activity

Biogenic PdNPs were tested for their ability to suppress butyrylcholinesterase (BChE) and acetylcholinesterase (AChE). The nanoparticles was discrete in PBS at (pH 8) and a concentration of 25–400 µg/mL against BChE and AChE. The inhibitory potential for enzymes was to be dose-dependent as illustrated in **(**Fig. 8**B)**. The highest inhibition was obtained for AChE (73.7 ± 1.61) and BChE (78.78 ± 0.21) with IC_{50} values of 288.2 and 269 µg/mL at 400 µg/mL, respectively (Fig. 8**B)**.

3.8.7. Anticancer activity

The anticancer activity of PdNPs was examined against MCF-7 and HCT-116 cell lines, as illustrated in (Fig. 9**A**). The IC_{50} value of Dox were 15.6 M (Fig. 9**a**) for MCF-7 and 9.8 M for HCT-116 (Fig. 9**d**). The IC_{50} of *Licorice root* extract against MCF-7 and HCT-116 was 160 (Fig. 9**b**) and 95.5 µg/mL (Fig. 9**e**). The IC_{50} of PdNPs and *Licorice root* extract against MCF-7 and HCT-116 was 44.4 (Fig. 9**c**) and 6.58 µg/mL (Fig. 9**f**) respectively. The increased cytotoxicity (Fig. 9 **b, e**) and decreased cell proliferation percentages (Fig. 9 **a, d**) of MCF-7 and HCT-116 were observed. The cytotoxicity of *licorice root* extract, Dox, and PdNPs was investigated using fluorescence-activated cell sorting on MCF-7 cells for 24 h. The activity of *Licorice root* extract (40 mM) and Dox (10 mM) was increased. The mixture of licorice root extract and dox significantly

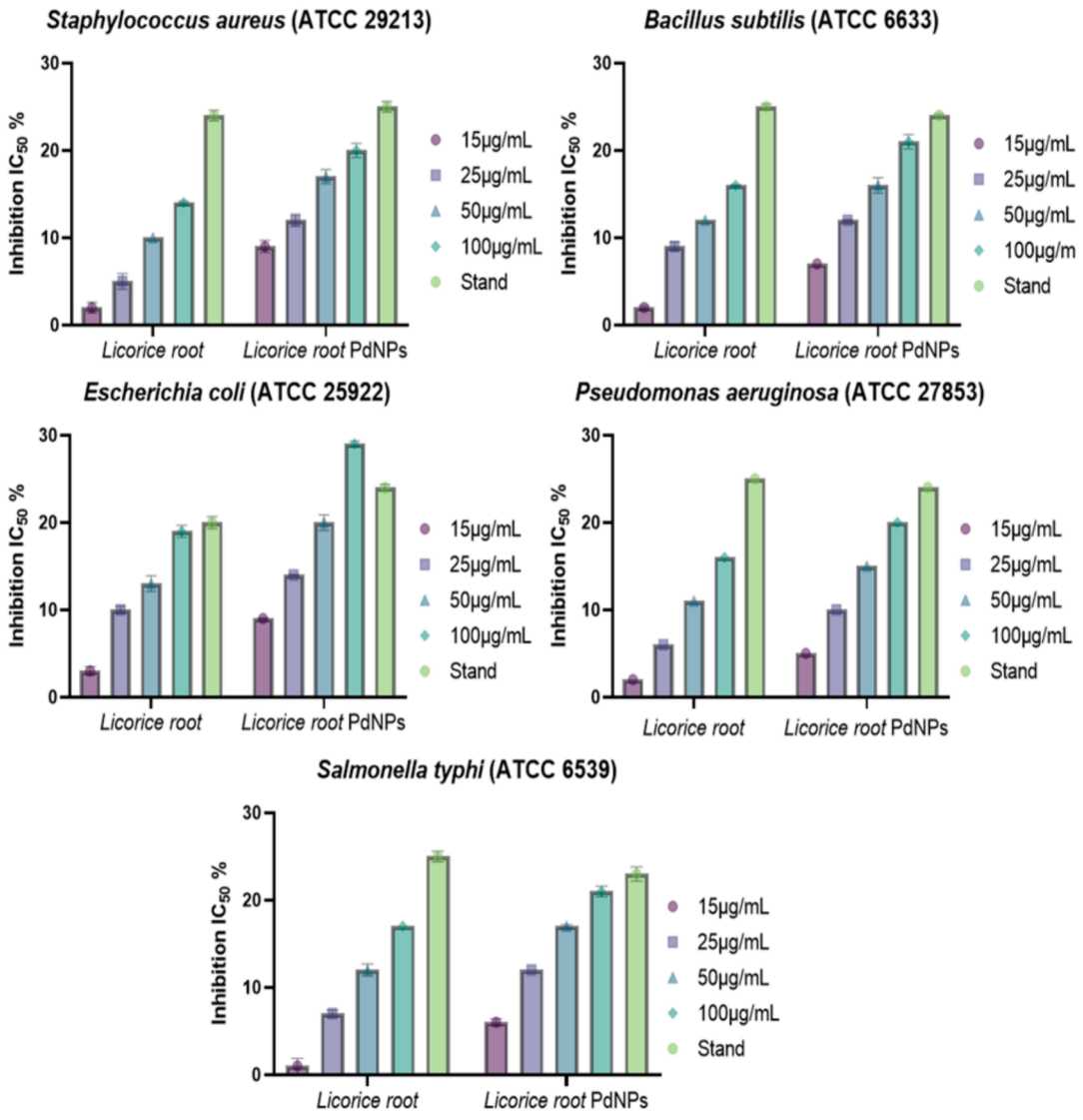

Fig. 7. Antibacterial potential of PdNPs against *Staphylococcus aureus*, *Escherichia coli*, *Pseudomonas aeruginosa*, and *Bacillus subtilis*.

increased overall annexing cells in contrast to the control group ($P < 0.001$), (Fig. 9**B**). The HCT-116 cells revealed substantial increase in annexing-positive cells after treatment with licorice root extract (40 mM), dox (10 mM), and both together for 24 h compared to the control group. The MCF-7 and HCT-116 cells treated with *licorice root* extract and Dox showed significantly higher caspase 3 activity in contrast to the control group ($P < 0.001$). Additionally, the HCT-116 ($P < 0.001$) and MCF-7 ($P < 0.001$) handled with *licorice root* extract + Dox had considerably higher caspase 3 activity compared to the control (Fig. 9**B**).

4. Discussions

The study synthesizes PdNPs using licorice root, demonstrating their potential applications in medicine and electronics. Different techniques were used to characterize the PdNPs including UV–vis, TEM, EDX, XRD, and FTIR. PdNPs were synthesized by mixing Pd salt with (4 mL) *licorice root* extract which turned dark brown with the Pd^{+2} ion peak fading after three hours which was confirmed through UV–Vis spectroscopy (Basavegowda et al., 2015). TEM images revealed cylindrical PdNPs with randomly oriented nanoparticle scattering due to the aggregation of tiny 1–20.22 nm particles (Khan et al., 2017; Cookson, 2012).

The FTIR analysis revealed that polyphenols and alkaloids are key indicators that were confirmed by a peak at 544 cm^{-1} for NPs synthesis (Han et al., 2019). The phytoconstituents present in *licorice root* extract are triterpenoids, flavonoids, and steroids that exhibit strong reducing ability aiding in the reduction and stabilization of nanoparticles. The exact mechanism of PdNP biogenic synthesis is still unclear, however three main steps have been proposed. Initially, electrons from a donor metabolite must be obtained in order to reduce Pd^{2+} ions to Pd^{0}. The reduced ions then nucleate, grow, and clump together to form PdNPs that are thermodynamically stable. Lastly, the nanoparticles are capped by functional groups such as Glycyrrhizin, licochalcone A, 18β-glycyrrhetinic acid, glabridin, liquiritigenin, and licochalcone that are responsible for the stabilization of nanoparticles. The X-ray diffraction analysis revealed a strong Pd band at (1 1 1) indicating the crystalline nature of PdNPs (Sriramulu and Sumathi, 2018., Al-Ahmed et al., 2020).

The EDX analysis revealed a strong peak at 2.8 kV, confirming the presence of PdNPs and carbon and oxygen, possibly due to plant biomolecules capping and reducing Pd ions. The charge distribution or Zeta potential of nanoparticles confirmed their effective toxicity against microorganisms and cancerous cell lines (Basavegowda et al., 2015). X-ray photoelectron spectroscopy analysis revealed PdNPs binding energies at 340.99–337.15 eV with a 3.84 eV band gap, indicating Pd (II) was reduced to Pd (0) (Al-Radadi., 2022e).

The study found that antioxidant activity showed maximum

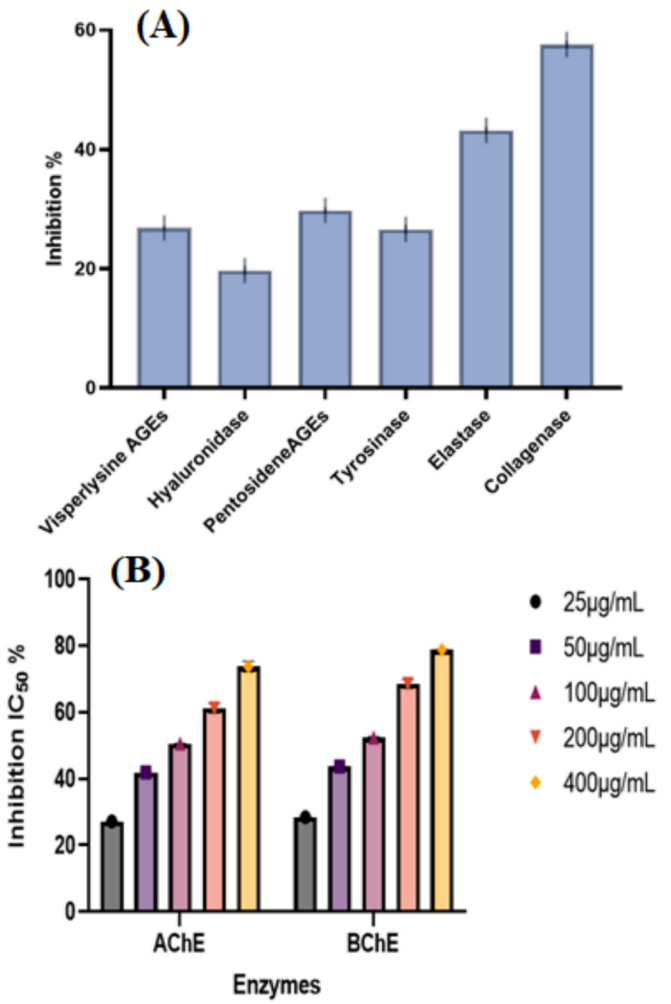

Fig. 8. Anti-aging potential of PdNPs **(A)**, Anti-Alzheimer's potential at varying concentrations of PdNPs **(B)**.

inhibition in extracts against DPPH and ABTS free radicals at 100 µg/mL of PdNPs. *Licorice roots* contain phenolic and ascorbic acid, which contribute electrons and hydrogen atoms to actively quench ABTS and DPPH radicals. Further, the small size (1–10 nm) exhibits superior antioxidant activity (60 %) indicating their superiority at lower nanoparticle doses (Yeo and Shahidi, 2019). Similar data reports the DPPH assay against biosynthesized lead oxide nanoparticles which demonstrates 58 % DPPH radical scavenging at 200 µg/mL concentrations. Likewise, SeNPs assimilate into selenoproteins that increase antioxidant activities and reduce inflammatory responses (Al Jahdaly et al., 2021).

PdNPs showed dose-dependent anti-inflammatory activity, with 80.42 % and 95.01 % activity at concentrations of 50 and 100 µg/mL, respectively. Thus, the study reveals that the anti-inflammatory activity of PdNPs is size-dependent and can be increased with concentrations ranging from 0 to 50 µg/mL, indicating 10–87 % anti-inflammatory activity (Mohana and Sumathi, 2020). Similary, metal and oxide nanoparticles have been found to possess anti-inflammatory properties that significantly reducing VEGF levels act as a key factor in antigen sensitization and physiologic dysregulation (Sheikpranbabu et al., 2009, Abdullah et al., 2022., Faisal et al.,2021).

PdNPs show significant antimicrobial potential against *Pseudomonas aeruginosa*, *Escherichia coli*, and *Salmonella typhi* at concentrations of 18–100 µg/mL, but no studies on environmentally friendly production using *licorice root* extract. Similarly, ZnO, CuO, and Fe_2O_3 nanoparticles showed potent antimicrobial action against Gram-positive and Gram-negative bacteria (Azam et al., 2012, Al-Radadi et al., 2022). In the antileishmanial activity of nanoparticles, the maximum inhibition obtained was 69 ± 0.25 for *promastigote* and 77 ± 0.10 % for *amastigote* at 400 µg/mL, respectively. The data suggests the concentration dependent leishmania and cytotoxic activity which also showed that the amastigotes parasite being more sensitive to nanoparticles. Tyrosinase deficiency is linked to aging, freckles, and pigmentary, malignant melanoma disorder.

PdNPs significantly inhibited tyrosinase (26.6 ± 0.82 %) and collagenase (57.6 ± 0.61 %) at 400 µg/mL in an antiaging assay, with the lowest activity observed for hyaluronidase (19.70 ± 0.83 %) (Jan et al., 2020). The biosynthesized PdNPs exhibit strong tyrosinase inhibitory activity, in accordance with recent reports on tyrosinase inhibition using metal nanoparticles (Aberg et al., 2004). Several synthetic and biological compounds have been used in recent therapeutic interventions to inhibit the cholinesterase enzymes that cause Alzheimer's disease (Al-Radadi 2022b). PdNPs are neurotoxic, blocking cholinesterase receptors, with IC_{50} values of 269 and 288.2 µg/mL for BChE and AChE, respectively.

The study evaluated the significant anti-angiogenic and anticancer properties against *licorice root* extract, Dox, and a combination of both in joint therapy for MCF-7 and HCT-116 (Al-Radadi., 2021a, Al-Radadi., 2021b). PdNPs demonstrated potent anticancer activity against cell lines of MCF-7 and HCT-116, with decreased cell proliferation at high concentrations, aligning with previous reports on anti-angiogenic activity (Kıyan, 2023). So, *Licorice root* extracts are rich in flavonoids and glycyrrhizin that have potential applications in nanoparticle synthesis and pharmaceuticals due to their therapeutic properties, prompting an urgent need for research on developing natural Glycyrrhiza ingredients.

5. Conclusion

The green synthesis of PdNPs is the most accurate, simple, and environmentally sustainable procedure. The current study demonstrates the biosynthesis of PdNPs which was confirmed by using different techniques. The optimal synthesis of PdNPs was achieved by a temperature of 100 °C using *licorice root* extract with an absorbance peak of 370 nm. The XRD analysis revealed the crystallinity and TEM images confirmed spherical morphology with size ranges of 1.2–10 nm. XPS peaks at 534.2, 401.35, and 286.71 eV were assigned to O1 s, N1 s, and C1 s, respectively. Moreover, the synthesized nanoparticles exhibited potent antibacterial, anti-leishmanial, anti-Alzheimer, antiaging, antioxidant, and anticancer activity.

6. Future perspectives

The physiochemical characterizations of *Licorice root*-PdNPs present promising biomedical applications, including targeted drug delivery and reduced side effects. PdNPs revealed novel cancer therapeutics due to their anti-proliferative activity, and their potent antibacterial activity could help to combat drug-resistant infections. The synthesized PdNPs showed maximum anti-Alzheimer and antioxidant potentials that demonstrate significant advancement in the environmentally friendly synthesis of nanoparticles. Thus, future research should explore optimization, alternative synthesis sources, and environmental impact of PdNPs which hold significant potential for advancing biomedical technologies and improving human health (Al-Radadi et al., 2022e).

CRediT authorship contribution statement

Najlaa S. Al-Radadi: Writing – review & editing, Writing – original draft, Visualization, Validation, Supervision, Software, Resources, Project administration, Methodology, Investigation, Funding acquisition, Formal analysis, Data curation, Conceptualization.

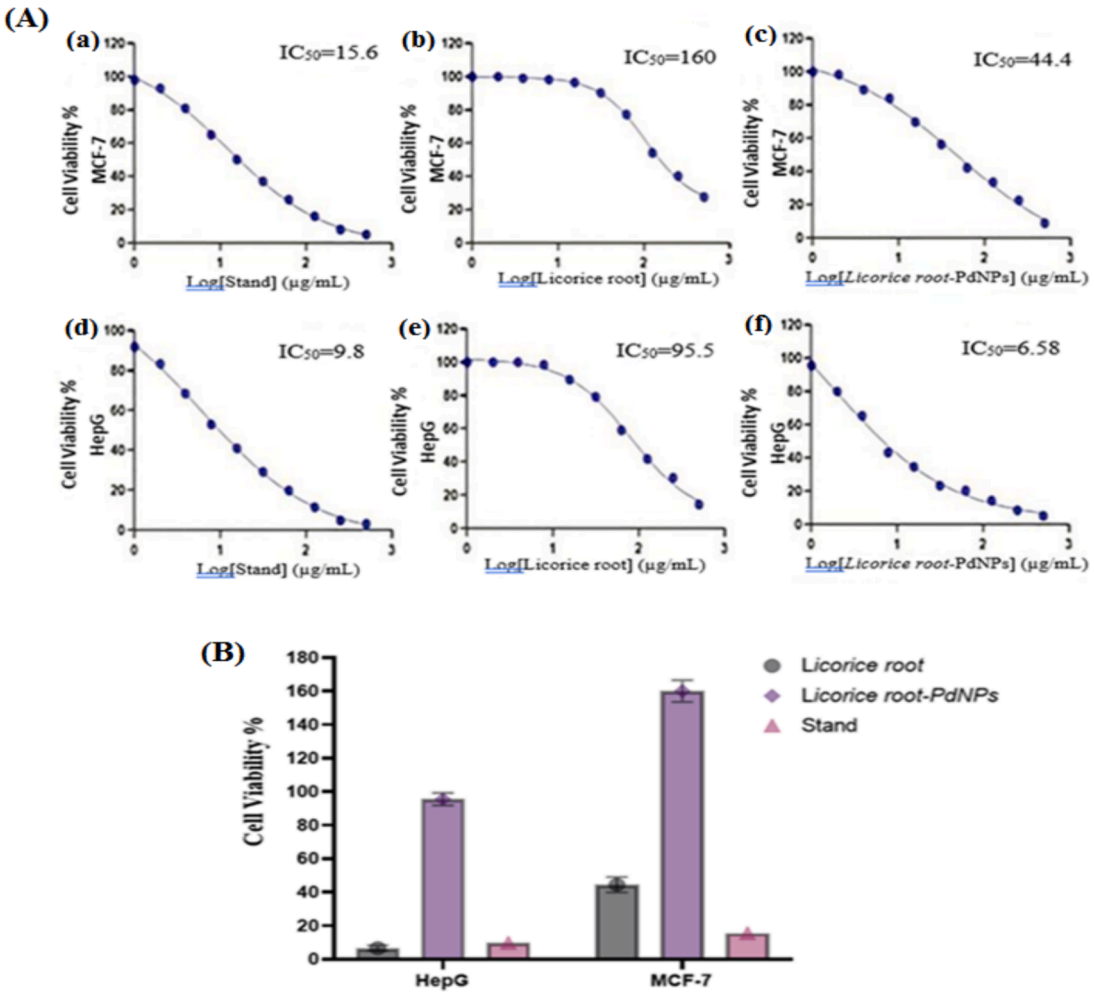

Fig. 9. Anticancer, The dose-dependent curves for standard, Glycyrrhiza and PdNPs (MCF-7 and HepG-2. Nonlinear regression was used to calculate the IC50 values, which were calculated as log (inhibitor) vs. response-variable slope. The error bars bars are expressed in Arithmetic means ± Standard deviation (A), MCF-7, HepG-2 cell lines cell viability and inhibition by PdNPs (B).

Declaration of competing interest

The authors declare that they have no known competing financial interests or personal relationships that could have appeared to influence the work reported in this paper.

References

Abdullah, Al-Radadi, N. S., T. Hussain, S. Faisal, et al., 2022, Novel biosynthesis, characterization and bio-catalytic potential of green algae (Spirogyra hyalina) mediated silver nanomaterials. Saudi J. Biol. Sci. 29 (1) 411-419.

Aberg, C.M., Chen, T., Olumide, A., et al., 2004. Enzymatic grafting of peptides from casein hydrolysate to chitosan. Potential for value-added byproducts from food-processing wastes. J. Agric. Food Chem. 52 (4), 788–793.

Al Jahdaly, B.A., Al-Radadi, N.S., Eldin, G.M., et al., 2021. Selenium nanoparticles synthesized using an eco-friendly method: dye decolorization from aqueous solutions, cell viability, antioxidant, and antibacterial effectiveness. J. Mater. Res. Technol. 11, 85–97.

Al-Ahmed, Z.A., Al-Radadi, N.S., Ahmed, M.K., Shoueir, K., El-Kemary, M., 2020. Dye removal, antibacterial properties, and morphological behavior of hydroxyapatite doped with Pd ions. Arab. J. Chem. 13 (12), 8626–8637.

Al-Radadi, N.S., 2018. Artichoke (Cynara scolymus L.), mediated rapid analysis of silver nanoparticles and their utilisation on the cancer cell treatments. J. Comput. Theor. Nanosci. 15 (6-7), 1818–1829.

Al-Radadi, N.S., 2019. Green synthesis of platinum nanoparticles using Saudi's Dates extract and their usage on the cancer cell treatment. Arab. J. Chem. 12 (3), 330–349.

Al-Radadi, N.S., 2021a. Facile one-step green synthesis of gold nanoparticles (AuNp) using licorice root extract: Antimicrobial and anticancer study against HepG2 cell line. Arab. J. Chem. 14 (2), 102956.

Al-Radadi, N.S., 2021b. Green biosynthesis of flaxseed gold nanoparticles (Au-NPs) as potent anti-cancer agent against breast cancer cells. J. Saudi Chem. Soc. 25 (6), 101243.

Al-Radadi, N.S., 2022a. Microwave assisted green synthesis of Fe@ Au core–shell NPs magnetic to enhance olive oil efficiency on eradication of helicobacter pylori (life preserver). Arab. J. Chem. 15 (5), 103685.

Al-Radadi, N.S., 2022b. Biogenic proficient synthesis of (Au-NPs) via aqueous extract of Red Dragon Pulp and seed oil: Characterization, antioxidant, cytotoxic properties, anti-diabetic anti-inflammatory, anti-Alzheimer and their anti-proliferative potential against cancer cell lines. Saudi J. Biol. Sci. 29 (4), 2836–2855.

Al-Radadi, N.S., 2022c. Laboratory scale medicinal plants mediated green synthesis of biocompatible nanomaterials and their versatile biomedical applications. Saudi J. Biol. Sci. 29 (5), 3848–3870.

Al-Radadi, N.S., 2022d. Single-step green synthesis of gold conjugated polyphenol nanoparticle using extracts of Saudi's myrrh: Their characterization, molecular docking and essential biological applications. Saudi Pharm. J. 30 (9), 1215–1242.

Al-Radadi, N.S., 2022e. Saussurea costus for sustainable and eco-friendly synthesis of palladium nanoparticles and their biological activities. Arabian Journal of Chemistry. Arab. J. Chem. 15 (11), 104294.

Al-Radadi, N.S., 2023. Ephedra mediated green synthesis of gold nanoparticles (AuNPs) and evaluation of its antioxidant, antipyretic, anti-asthmatic, and antimicrobial properties. Arab. J. Chem. 16 (1), 104353.

Al-Radadi, N.S., Abu-Dief, A.M., 2022. Silver nanoparticles (AgNPs) as a metal nano-therapy: possible mechanisms of antiviral action against COVID-19. Inorg. Nano-Met. Chem. 1–19.

Al-Radadi, N.S., Adam, S.I., 2020. Green biosynthesis of Pt-nanoparticles from Anbara fruits: Toxic and protective effects on CCl4 induced hepatotoxicity in Wister rats. Arab. J. Chem. 13 (2), 4386–4403.

Al-Radadi, N. S. and A. N. Al-Youbi, 2018a. One-step synthesis of au nano-assemblies and study of their anticancer activities. J. Comput. Theor. Nanosci. 15 (6-7) 1861-1870.

Al-Radadi, N. S., AlBishri, Widad, M., ElShebiney, Shaimaa A., and Salem, Neveen A., 2024. Plant-Mediated Green Synthesis of Gold Nanoparticles Using an Aqueous Extract of *Passiflora ligularis*, Optimization, Characterizations, and their

Neuroprotective Effect on Propionic Acid-Induced Autism in Wistar Rats. Saudi Pharm. J. 32 (2) 101921.
Al-Radadi, N.S., Faisal, S., Alotaibi, A., et al., 2022. Zingiber officinale driven bioproduction of ZnO nanoparticles and their anti-inflammatory, anti-diabetic, anti-Alzheimer, anti-oxidant, and anti-microbial applications. Inorg. Chem. Commun. 140, 109274.
Al-Radadi, N. S. and d. A. N. Al-Youbi, 2018b. Environmentally-safe synthesis of gold and silver nano-particles with AL-madinah Barni fruit and their applications in the cancer cell treatments. J. Comput. Theor. Nanosci. 15 (6-7) 1853-1860.
Azam, A., Ahmed, A.S., Oves, M., et al., 2012. Antimicrobial activity of metal oxide nanoparticles against Gram-positive and Gram-negative bacteria: a comparative study. Int. J. Nanomed. 6003–6009.
Basavegowda, N., Mishra, K., Lee, Y.R., 2015. Ultrasonic-assisted green synthesis of palladium nanoparticles and their nanocatalytic application in multicomponent reaction. New J. Chem. 39 (2), 972–977.
Cerqueira, B.B.S., Lasham, A., Shelling, A.N., et al., 2015. Nanoparticle therapeutics: Technologies and methods for overcoming cancer. Eur. J. Pharm. Biopharm. 97, 140–151.
Chakravarthi, K.K., Avadhani, R., 2013. Beneficial effect of aqueous root extract of Glycyrrhiza glabra on learning and memory using different behavioral models: An experimental study. J. Nat. Sci. Biol. Med. 4 (2), 420.
Cookson, J., 2012. The preparation of palladium nanoparticles. Platin. Met. Rev. 56 (2), 83–98.
Deplanche, K., Bennett, J., Mikheenko, I., et al., 2014. Catalytic activity of biomass-supported Pd nanoparticles: influence of the biological component in catalytic efficacy and potential application in 'green'synthesis of fine chemicals and pharmaceuticals. Appl. Catal. B: Environ. 147, 651–665.
Faisal, S., Al-Radadi, N.S., Hussain, T., Abdullah, et al., 2021. Curcuma longa Mediated Synthesis of Copper Oxide, Nickel Oxide and Cu-Ni Bimetallic Hybrid Nanoparticles: Characterization and Evaluation for Antimicrobial, Anti-Parasitic and Cytotoxic Potentials. Coatings 2021 (11), 849.
Goyal, P., Manzoor, M.M., Vishwakarma, R.A., et al., 2020. A comprehensive transcriptome-wide identification and screening of WRKY gene family engaged in abiotic stress in Glycyrrhiza glabra. Sci. Rep. 10 (1), 373.
Han, Z., Dong, L., Zhang, J., et al., 2019. Green synthesis of palladium nanoparticles using lentinan for catalytic activity and biological applications. RSC Adv. 9 (65), 38265–38270.
Jan, H., Khan, M.A., Usman, H., et al., 2020. The Aquilegia pubiflora (Himalayan columbine) mediated synthesis of nanoceria for diverse biomedical applications. RSC Adv. 10 (33), 19219–19231.
Khan, M., Kuniyil, M., Shaik, M.R., et al., 2017. Plant extract mediated eco-friendly synthesis of Pd@ graphene nanocatalyst: An efficient and reusable catalyst for the Suzuki-Miyaura coupling. Catalysts. 7 (1), 20.
Kıyan, H., 2023. Antioxidant and Antiangiogenic Effect of Homoleptic Palladium (II) Carboxamide Complex Loaded Chitosan Modified PLGA Nanoparticles: In vitro Evaluation and In vivo Chick Embryo Chorioallantoic Membrane (CAM) Assay. Lett. Drug Des. 20 (8), 1158–1170.
Mayedwa, N., Mongwaketsi, N., Khamlich, S., et al., 2018. Green synthesis of nickel oxide, palladium and palladium oxide synthesized via Aspalathus linearis natural extracts: physical properties & mechanism of formation. Appl. Surf. Sci. 446, 266–272.
Mohana, S., Sumathi, S., 2020. Multi-functional biological effects of palladium nanoparticles synthesized using Agaricus bisporus. J. Clust. Sci. 31, 391–400.
Perveen, R., Shujaat, S., Naz, M., et al., 2021. Green synthesis of antimicrobial silver nanoparticles with Brassicaceae seeds. Mater. Res. Express. 8 (5), 055007.
Sheikpranbabu, S., Kalishwaralal, K., Venkataraman, D., et al., 2009. Silver nanoparticles inhibit VEGF-and IL-1β-induced vascular permeability via Src dependent pathway in porcine retinal endothelial cells. J. Nanobiotechnology. 7, 1–12.
Sriramulu, M., Sumathi, S., 2018. Biosynthesis of palladium nanoparticles using Saccharomyces cerevisiae extract and its photocatalytic degradation behaviour. Adv. Nat. Sci.: Nanosci. Nanotechnol. 9 (2), 025018.
Thakur, A., Raj, P., 2017. Pharmacological perspective of Glycyrrhiza glabra Linn: A mini-review. J. Anal. Pharm. Res. 5 (5), 00156.
Wittschier, N., Faller, G., Hensel, A., 2009. Aqueous extracts and polysaccharides from liquorice roots (Glycyrrhiza glabra L.) inhibit adhesion of Helicobacter pylori to human gastric mucosa. J. Ethnopharmacol. 125 (2), 218–223.
Yeo, J., Shahidi, F., 2019. Critical re-evaluation of DPPH assay: Presence of pigments affects the results. J. Agric. Food Chem. 67 (26), 7526–7529.